Structural and electrical transport properties of superconducting $Au_{0.7}In_{0.3}$ films: A random array of superconductor–normal-metal–superconductor Josephson junctions

Yu. Zadorozhny and Y. Liu
Department of Physics, The Pennsylvania State University, University Park, Pennsylvania 16802
(Received 4 October 2001; revised manuscript received 30 April 2002; published 9 August 2002)

The structural and superconducting properties of $Au_{0.7}In_{0.3}$ films, grown by interdiffusion of alternating Au and In layers, have been studied. The films were found to consist of a uniform solid solution of $Au_{0.9}In_{0.1}$, with excess In precipitated in the form of In-rich grains of various Au-In phases with distinct atomic compositions, including intermetallic compounds. As the temperature was lowered, these individual grains became superconducting at a particular local transition temperature (T_c^0), determined primarily by the atomic composition of the grain, before a fully superconducting state of zero resistance was established. From the observed onset temperature of the superconducting transition, it was inferred that up to three different superconducting phases could have formed in these $Au_{0.7}In_{0.3}$ films, all of which were embedded in a uniform $Au_{0.9}In_{0.1}$ matrix. Among these phases, the T_c^0 of a particular one, 0.8 K, is higher than any previously reported for the Au-In system. The electrical transport properties were studied down to low temperatures. The transport results were found to be well correlated with those of the structural studies. The present work suggests that these $Au_{0.7}In_{0.3}$ films can be modeled as a random array of superconductor–normal-metal–superconductor Josephson junctions. The effect of disorder and magnetic field on the superconducting transition in these $Au_{0.7}In_{0.3}$ films is discussed.

DOI: 10.1103/PhysRevB.66.054512 PACS number(s): 74.40.+k, 74.76.Db

I. INTRODUCTION

The interplay between superconductivity and carrier localization has long been a focus of research on disordered superconductors. This question was initially raised in studies of granular superconducting films.[1] Such films, in which individual grains are separated by insulating barriers, can be modeled as superconductor-insulator-superconductor (SIS) tunnel junction arrays.[2] At lower temperatures, the film properties are dictated by the competition between intergrain Josephson coupling and carrier confinement due to the charging energy of the junctions. For a superconducting grain, the number of Cooper pairs and the phase of the superconducting order parameter are conjugate variables subject to an uncertainty relation.[3] As the fluctuation in the number of Cooper pairs is suppressed due to the charging energy, the fluctuation in the superconducting phase is enhanced. Josephson coupling between adjacent superconducting grains, if strong enough, will lead to global phase coherence.[4]

The localization effect has also been examined for homogeneously disordered systems, such as ultrathin amorphous films,[5] in which electrons in the normal state are strongly localized. In this case, superconductivity can also be suppressed, leading to a reduction in the superconducting transition temperature or a complete loss of superconductivity.[4] The same phase-number uncertainty relation can also be used to understand this phenomenon, since the fluctuation in the number of electrons is again suppressed, in this case due to localization. In fact, a theoretical model based on this picture has been suggested.[6] As the amount of disorder increases, a structurally and chemically homogeneous superconducting film will break down into superconducting droplets, linked by Josephson coupling. The superconducting state will survive only if the coupling is sufficiently strong. This model makes it possible to understand the interplay between superconductivity and localization in both granular and homogeneous films on the same footing.

A natural question to ask is whether it is possible to identify a system that can be disordered for superconductivity, but in which electrons or Cooper pairs are not particularly localized. An example of such a system could be a granular superconductor with a superconductor–normal-metal–superconductor (SNS) type of intergrain Josephson coupling. In this regard, it is interesting to note that while artificial proximity-coupled Josephson junction arrays[7] have been examined in some detail, including finite-size effects[8] and the effect of disorder,[9] granular materials that can be modeled as an SNS junction array, such as niobium nitride films,[10] have hardly been studied.

We have studied films of $Au_{0.7}In_{0.3}$. These films are strongly disordered as far as superconductivity is concerned due to a spatially varying local superconducting transition temperature T_c^0. (Phase separation in this binary alloy system is directly responsible for the spatially varying T_c^0, as shown below.) On the other hand, Cooper pairs are not confined as in the case of conventional SIS granular films. We report several generic features of these $Au_{0.7}In_{0.3}$ films, grown at ambient temperature, in which the interdiffusion of Au and In led to the formation of several superconducting Au-In minority phases, including solid solutions and intermetallic compounds with distinct concentrations of Au and In. We show that these Au-In films may be regarded as random arrays of SNS junctions with unique superconducting properties. The morphology, chemical composition, and low-temperature electrical transport and superconducting properties of the system were found to be well correlated.

The rest of the paper is organized as follows: in Sec. II we review various phases present in bulk Au-In alloy and summarize the results on superconductivity in the Au-In binary system previously reported in the literature. In Sec. III we

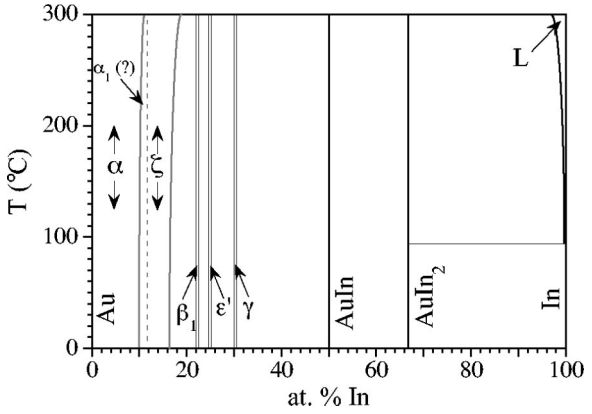

FIG. 1. Schematic Au-In phase diagram, after Ref. 11. Phases reported to be superconducting include pure In ($T_c = 3.4$ K), $AuIn_2$ ($T_c = 0.1$–0.2 K), AuIn ($T_c = 0.4$–0.6 K (however, the structure and phase composition were not determined; see text), ζ ($T_c \approx 0.1$ K), and α ($T_c = 0$–77 mK).

describe the techniques used in film growth and characterization. Sections IV and V deal with the film morphology and chemical composition. Sections VI and VII contain results on the electrical transport and superconducting properties of these films. Finally, Sec. VIII summarizes the results.

II. Au-In ALLOY

The phase diagram of the Au-In binary alloy system is rich and relatively well studied.[11] In the bulk form, the following alloy or intermetallic compound phases, stable at room temperature, have been reported:[11] (1) face-centered-cubic (fcc) solid solution with room-temperature solubility ranging from 0 to approximately 10 at. % of In (α phase); (2) the Nd- or Ni_3Ti-type hexagonal α_1 phase (11%–13% of In) (however, the existence of this phase as a stable one was questioned[11]); (3) close-packed-hexagonal (cph) solid solution (ζ, 10%–16% of In); (4)–(6) solid solution phases of β_1, ϵ', and γ', with In concentrations around 22%, 25%, and 30%, respectively (the structure and precise stoichiometries of these phases are yet to be clarified[11]); (7),(8) intermetallic compounds AuIn (triclinic) and $AuIn_2$ (of fluorite-type crystal structure) with a negligible solubility of In or Au in these compounds. There is no appreciable solid solubility of Au in In. A schematic phase diagram around room temperature is shown in Fig. 1, in which the α_1 phase is marked with a dashed line to reflect the uncertainty associated with this phase. In thin-film samples prepared by interdiffusion of Au and In at room temperature, a technique employed in the present experiment, additional phases may be present due to substrate effects, before the thermal equilibrium is reached.

Superconductivity in several phases of Au-In alloy has been reported, as summarized in Ref. 11. In bulk form, pure In has a transition temperature of 3.40 K. The T_c of the intermetallic compound AuIn was reported to be between 0.4 K and 0.6 K.[12] However, the measurements were done on powdered samples, without any structural characterization. The phase composition of the sample—in particular, whether the sample was of a single phase—was not verified. As a result, the T_c of AuIn should be considered unsettled. Our measurements appeared to indicate that the superconducting transition temperature of a AuIn phase might be higher than 0.6 K (see below). Measurements on $AuIn_2$ ingots yielded values of T_c from 0.1 K (Ref. 13) to 0.2 K (Ref. 14). For the α phase, the T_c of $Au_{0.9}In_{0.1}$, close to the limit of solid solubility of In in Au, was 77 mK.[15] It further decreased to 11 mK for $Au_{0.94}In_{0.06}$ (Ref. 16) and to 0.5 mK for $Au_{0.98}In_{0.02}$ (Ref. 15). The T_c of the ζ phase has been reported to be between 35 and 100 mK for a nominal composition of $Au_{0.84}In_{0.16}$.[17]

From these previous studies it is clear that there exist numerous superconducting phases in the Au-In alloy system. In addition, a significant range of In concentration does not correspond to any single equilibrium phase at room temperature. As a result, depending on the composition and preparation technique, various phase-separated samples, possibly with metastable phases, are expected. Since a wide range of superconducting transition temperatures is possible for these phases, the local T_c^0 is expected to vary spatially as well.

The Au-In system has been of great interest for both fundamental research and practical applications. In particular, it has served as a model system for experimental studies of bulk and film solid diffusion and compound formation.[18–21] The α-phase alloy attracted a large amount of attention in the pursuit of possible superconductivity in pure Au.[15,16] Nuclear ferromagnetism was recently found to coexist with superconductivity in $AuIn_2$ at microkelvin temperatures.[22] Au-In alloy wets most of the substrates commonly used, with a long superconducting coherence length even in thin-film form. It has been used to fabricate ultrathin (≈ 150 nm in diameter) superconducting cylinders on quartz filaments, with a phase diagram that features multiple superconducting regions.[23] We have previously reported observations of strongly enhanced magnetic fingerprints[24] and of fractional-flux Little-Parks oscillations[25] in disordered mesoscopic $Au_{0.7}In_{0.3}$ cylinders.

Au-In alloy is also important for practical applications. The wide range of superconducting transition temperatures in the same material system is useful for applications where a particular T_c is needed. Au-In films are structurally stable, easy to prepare, and do not oxidize significantly. $AuIn_2$, in particular, has been used in commercial superconducting quantum interference devices (SQUID's).

III. SAMPLE PREPARATION AND MEASUREMENTS

Au-In films were deposited at ambient temperature in high vacuum ($<10^{-6}$ mbar) by back-to-back thermal evaporation of 99.9999% pure Au and In. The two tungsten-coil sources, separated by a shield, were 8 cm apart and 25 cm away from the substrate. Glazed alumina or polished quartz was used as substrates. Three or five alternating layers were deposited, the top and the bottom layers being Au. The respective layer thicknesses for Au and In, not exceeding 10 nm each, were determined based on the desired stoichiometric ratio. During evaporation, the deposition rate was controlled using a quartz crystal thickness monitor. A typical film was 6 mm long and 0.5 mm wide, patterned by a

shadow mask for four-point electrical transport measurements.

The initial mixing of Au and In apparently occurred during the evaporation, at the ambient temperature. Subsequent interdiffusion continued at room temperature. Based on a previous study, the film structure should stabilize within several days.[19] Depth profiles of $Au_{0.7}In_{0.3}$ films revealed signs of incomplete interdiffusion of Au and In right after the deposition. However, they became undetectable after a few days (Sec. V). Resistance measurements showed no evidence for a superconducting transition at 3.4 K in any film, indicating that no macroscopic fraction of pure In was present.

The surface of every Au-In film was studied by atomic force microscopy (AFM) and/or by scanning electron microscopy (SEM). X-ray photoelectron spectroscopy (XPS) was used to probe the vertical chemical composition profile of selected samples. The relative concentrations of Au and In were inferred from the energy spectra of emitted electrons, averaged over a surface area of the order of 1 mm^2 and a depth of about 5 nm. After each scan, the surface layer was removed by Ar^+ ion etching, exposing the underlying material. A depth profile of the chemical composition was generated by repeating this procedure until all of the film was etched away. Limited laterally resolved, depth-averaged composition analysis was carried out using backscattered electron micrography (BSEM) and characteristic x-ray analysis. The crystalline structure of the films was also analyzed by x-ray diffractometry (XRD).

Electrical transport measurements of Au-In films were carried out in a ^{3}He or a dilution refrigerator equipped with a superconducting magnet. All electrical leads entering the cryostat were filtered with the attenuation of 10 dB at 10 MHz and 50 dB at 300 MHz. The resistance of the films was measured using a dc current source and a digital nanovoltmeter in a four-wire configuration. The bias current was chosen in the Ohmic regime of the current-voltage (I-V) characteristic (typically 1 μA).

IV. FILM MORPHOLOGY

It is known that film morphology for a particular material system can vary widely depending on the preparation conditions. For $Au_{0.7}In_{0.3}$ films, it was found that, depending on the evaporation rate (e) and the total thickness (d), two types of $Au_{0.7}In_{0.3}$ films, marked by their distinct surface morphology, could be grown.

Films thinner than 30 nm ($d<30$ nm) were found to be smooth, regardless of the evaporation rate ($0.1 \leqslant e \leqslant 2$ nm/s). Thick films ($d \geqslant 30$ nm) were also smooth if deposited at 0.5 nm/s or slower. However, micron-size grain clusters were found in thick films that had been deposited at 1–2 nm/s, resulting in bumpy films. The change in the film morphology for thicker films may be attributed to the higher atomic mobility during fast deposition. In thinner films, the formation of clusters was suppressed probably because of the reduced atom mobility originating from substrate effects.

AFM pictures of two $Au_{0.7}In_{0.3}$ films are shown in Fig. 2. Film No. 25, nominally 7.5 nm thick, represents the smooth films. The film was indeed uniform at large length scales, as seen in Fig. 2(a). A close-up view [Fig. 2(b)] revealed the presence of grains with a typical size of 20 nm, larger than the nominal film thickness. This may indicate that the film was formed by a single layer of grains. The grains were most likely crystalline, according to XRD studies of thicker $Au_{0.7}In_{0.3}$ films.

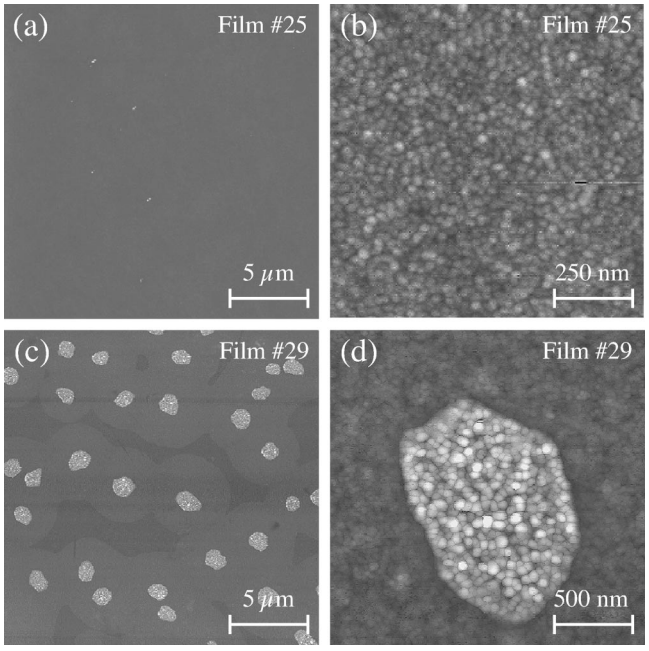

FIG. 2. AFM images of two $Au_{0.7}In_{0.3}$ films. Brighter areas correspond to more elevated regions. (a),(b) are for a 7.5-nm-thick sample, film No. 25. Image areas are 20×20 and 1×1 μm^2, respectively. Image depth, the surface height variation corresponding to the entire gray scale, is 5 nm for both pictures. (c),(d) are for a 40-nm-thick (film No. 29). Image areas 20×20 and 2×2 μm^2, respectively, with an image depth of 100 nm.

A 40-nm-thick sample, film No. 29, shown in Figs. 2(c) and 2(d), a representative of bumpy films, was prepared by depositing at a rate greater than 1 nm/s. For such films, the variation in the surface height was comparable to the total film thickness. Distinct clusters, seen as bright spots in the picture, protruded from the rest of the film surface by about 20 nm. The clusters, several microns apart, often appeared to have a somewhat rounded hexagonal shape, with a typical size of 1 μm. The clusters were surrounded by circular terraces, which were 4–5 μm in diameter and elevated above the rest of the film by a few nm.

A closer examination [Fig. 2(d)] revealed that the size of the grains in the clusters is approximately 60 nm, while the grains comprising surrounding areas were similar in size to those in uniform films. This might be a consequence of the larger film thickness at the protruding clusters or an indication that the clusters were of a Au-In phase different from that of the surrounding area.

V. PHASE COMPOSITION

Important questions are raised regarding the spatial variation of the chemical composition of the $Au_{0.7}In_{0.3}$ films and whether the local chemical composition correlates with the

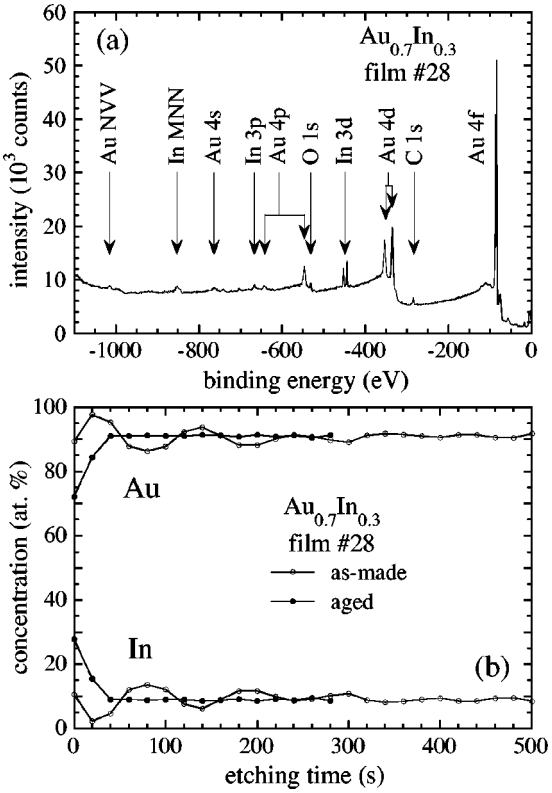

FIG. 3. (a) Photoelectron spectrum of the surface layer of a 100-nm-thick $Au_{0.7}In_{0.3}$ sample, film No. 28. Major lines are identified. (b) Depth profiles of the relative concentrations of Au and In for film No. 28. The concentrations are plotted as a function of the etching time (see text), which is proportional to the depth. Open circles, immediately after deposition; solid circles, about 2 months after the deposition.

film morphology. To answer these questions, depth profiling of the chemical composition was carried out by XPS. The XPS analysis yielded direct information on the chemical composition in the vertical direction of the film. When combined with AFM imaging, the XPS depth profiling also provided information on chemical composition in the lateral direction, as shown below.

A 100-nm-thick sample with large surface area (film No. 28) was prepared for this purpose by alternate evaporations of six 10-nm-thick layers of Au and five 8-nm-thick layers of In onto a quartz substrate. An XPS depth profiling analysis was carried out immediately after the film deposition. Figure 3(a) contains an energy spectrum of photoelectrons emitted from the film's original surface. Au and In concentrations were calculated from the areas of Au $4p_{3/2}$ and In $3d_{5/2}$ lines, using standard sensitivity factors of 3.8 and 0.62, respectively. Traces of oxygen and carbon were found at the surface, likely due to post-deposition contamination in the air, but disappeared as the XPS analysis was carried out deeper into the film.

Shown in Fig. 3(b) are two depth profiles of film No. 28, obtained by taking XPS scans at approximately 4 nm steps. For the profile taken immediately after the deposition, remnants of the layers are evident near the surface but become less distinct as the substrate is approached. This can be understood by noting that the bottom layers, deposited first, were exposed to elevated temperatures during evaporation for longer times and therefore had interdiffused more. In the depth profile obtained after the film had been aged about 2 months, no evidence of any layered structure was found. The measured In concentration was approximately 28% at the surface of the film and 10% deep in the film.

The above observation can be explained by taking into account the ion etching rate for different alloy phases. In Fig. 4, we show a sequence of AFM scans of the film's surface at different stages of profiling. The surface roughness increased significantly after etching, suggesting that the In-rich grains were preferentially sputtered away during ion etching, leaving behind the In-deficient matrix. Indeed, XPS could only detect the $Au_{0.9}In_{0.1}$ component after two or three etching cycles, in agreement with this preferential etching picture. Taking into account the bulk phase diagram described above, it is clear that the uniform matrix was the saturated solid solution, $Au_{0.9}In_{0.1}$ (α) phase. An XPS scan of the original film surface yielded an In concentration close to the nominal composition value of 30%. The difference between the measured In concentration and the expected $Au_{0.7}In_{0.3}$ composition at the film surface, particularly evident in the earlier depth profile, could be due to the incomplete interdiffusion of Au and In in the surface layer, with Au being the ending layer.

The electrical transport measurements, discussed below, suggested that the In-rich grains found in $Au_{0.7}In_{0.3}$ films might be made of different phases, including the intermetallic compound AuIn. A previous study of the room-temperature interdiffusion of Au and In in Au-In bilayers[19] showed that for an In fraction between 23% and 36%, both AuIn and $AuIn_2$ compounds were formed initially in the excess Au. However, after several days and for months thereafter, only AuIn could be found. If the same pattern of phase formation is applicable to our three- or five-layer films, then the In-rich grains might predominantly be the intermetallic compound AuIn.

The presence of protruding clusters in the bumpy films is

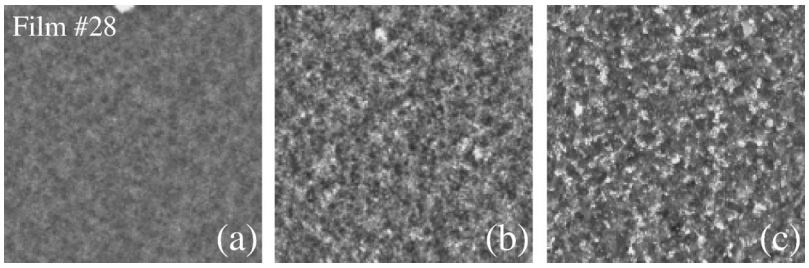

FIG. 4. AFM images of film No. 28 at different stages of depth profiling: (a) before ion etching, (b) with ≈ 5 nm removed, and (c) with ≈ 50 nm removed. All pictures are 10×10 μm^2, with an image depth of 100 nm. Preferential sputtering of the In-rich phase is evidenced by the surface roughening of the process.

very striking. Could the chemical composition of these clusters be different from the rest of the film? XPS studies of these bumpy films yielded depth profiles similar to those described above. Most importantly, the protruding clusters did not appear to be preferentially etched by Ar^+ ions. Therefore these clusters were likely *not* the same In-rich phases found in the uniform $Au_{0.9}In_{0.1}$ matrix. The AFM images away from the clusters showed features similar to those in Fig. 4, suggesting that away from the clusters, bumpy films had a compositional distribution similar to the smooth films. While BSEM, characteristic x-ray analysis, and XRD were all attempted, the precise chemical composition and crystalline structure of the protruding clusters could not be determined from the complicated spectra obtained in the above analyses, mainly due to the lack of reliable standards. To determine the precise phase of these clusters, consideraby more work on crystallography of the Au-In system, including the preparation of single-phase samples to be used as standards, would be needed. These experiments, which are beyond the scope of the present study, were not carried out.

The picture emerging from these morphological and structural studies is that multiple material phases were formed in the films. The predominant phase appears to be the saturated $Au_{0.9}In_{0.1}$ (α) phase. The others were various In-rich phases. The $Au_{0.9}In_{0.1}$ formed a matrix with In-rich regions embedded in it randomly, in both the position and size.

VI. ELECTRICAL TRANSPORT AND SUPERCONDUCTING PROPERTIES

The characteristic features in film morphology and chemical composition are expected to dictate the electrical transport properties of the films. In Fig. 5 we show the normalized resistance plotted against temperature for two sets of $Au_{0.7}In_{0.3}$ films of varying thickness. In each set, the films were grown under the same nominal conditions except for a slight variation in the evaporation rate. The films in Fig. 5(a) were prepared by slow deposition ($e \leqslant 0.5$ nm/s), with all films exhibiting a smooth morphology, free of the protruding clusters. The films shown in Fig. 5(b) were prepared by fast deposition ($e > 0.5$ nm/s). Protruding clusters such as those shown in Figs. 2(c) and 2(d) were clearly evident in fast-deposited films with thicknesses of 30 nm and greater.

Physical insight may be obtained by examining the systematic behavior in the temperature dependence of the measured resistance. Films prepared by slow deposition, shown in Fig. 5(a), had three onset superconducting transition temperatures at roughly 0.45 K, 0.65 K, and 0.8 K, depending on film thickness. On the other hand, for films prepared by fast deposition, shown in Fig. 5(b), the onset of superconductivity was found only at 0.45 K and 0.8 K, with a sharp drop in film resistance around 0.6 K, roughly the onset T_c of 0.65 K observed in films prepared by slow deposition. For films of multiple phases, the onset of the superconducting transition usually marks the highest local T_c for a particular phase. Therefore these various onset temperatures observed in films shown in Fig. 5 may be interpreted as the T_c's of different In-rich phases.

The onset T_c's of 0.45 K and 0.65 K are consistent with

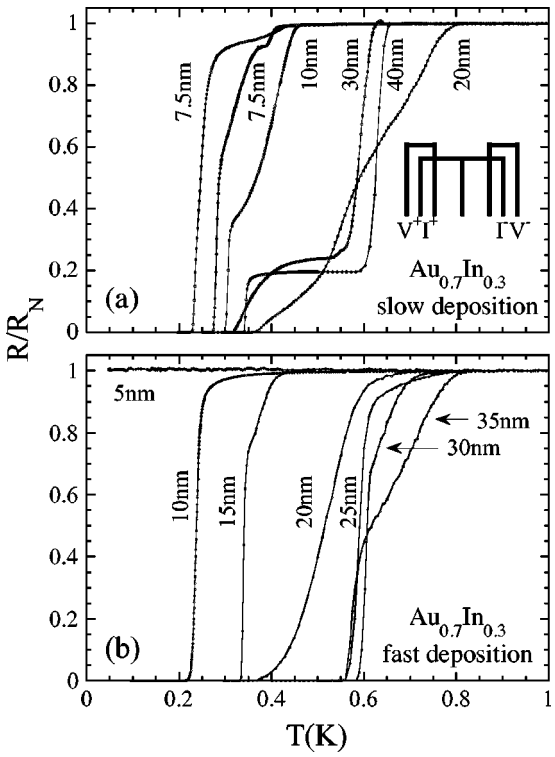

FIG. 5. Normalized resistance plotted as a function of temperature for two sets of $Au_{0.7}In_{0.3}$ films of varying thickness. (a) Films grown by slow deposition ($e < 0.5$ nm/s). The thicknesses are 7.5 nm (film No. 18 with $T_c = 0.229$ K and No. 25 with $T_c = 0.273$ K), 10 nm (film No. 24), 20 nm (film No. 23), 30 nm (film No. 22), and 40 nm (film No. 21). (b) Films grown by fast deposition ($e > 0.5$ nm/s). The film thicknesses are 5 nm (film No. 19), 10 nm (film No. 17), 15 nm (film No. 16), 20 nm (film No. 9), 25 nm (film No. 11), 30 nm (film No. 8), and 35 nm (film No. 10), as indicated. The two thickest films prepared by fast deposition contained protruding clusters. The film parameters are shown in Table I.

the T_c reported for a Au-In sample with a composition of AuIn.[12] Combining results obtained in the previous studies and our own morphological and compositional analyses presented above, it may be reasonable to conjecture that these two phases with onset T_c's of 0.45 K and 0.65 K represent two distinct In-rich phases embedded in the uniform $Au_{0.9}In_{0.1}$ (α) phase, possibly having the same chemical composition, AuIn, but different structural characteristics, resulting in different values of T_c.

The phase responsible for superconductivity at 0.8 K has not been previously reported for the Au-In system. Given that the onset T_c of 0.8 K appeared to be characteristic of the bumpy films, it might be possible that 0.8 K corresponds to the superconducting transition of the protruding clusters. This is consistent with the conjecture that the protruding clusters are of a phase *different* from the In-rich phases embedded in the α-phase matrix (with T_c's of 0.45 K and 0.65 K) with a nominal composition of AuIn as we argued above.

The above conjecture on the $T_c = 0.8$ K phase is supported by the observation of systematic behavior in $R(T)$ seen in thick $Au_{0.7}In_{0.3}$ films ($d \geqslant 30$ nm) prepared by fast

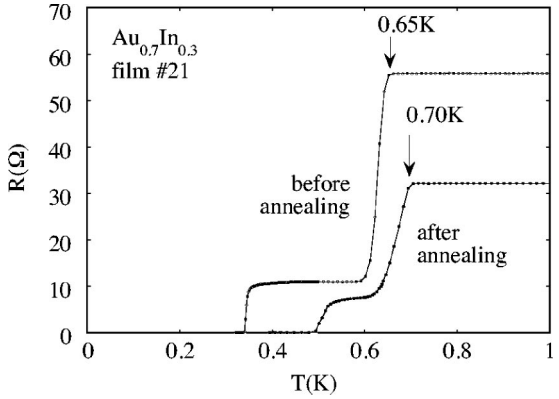

FIG. 6. Resistance plotted as a function of temperature for film No. 22 before (left curve) and after annealing (right curve). The shift in the onset T_c is indicated.

deposition. There was a gradual decrease in film resistance right below the onset $T_c = 0.8$ K, seen in Fig. 5(b). As the temperature was lowered, a sharp drop to zero resistance was found at $T = 0.6$ K. This can be easily understood if the local T_c of the protruding clusters is 0.8 K. In this picture, the protruding clusters induced superconductivity in their surrounding regions, consisting of the AuIn phases (T_c's of 0.45 K and 0.65 K) embedded in the uniform α-phase ($T_c = 77$ mK) matrix, due to the proximity effect. The size of these superconducting regions increased with decreasing temperature, resulting in a gradual drop in film resistance. As the temperature approaches 0.65 K, a zero-resistance superconducting state was established due to the emergence of global phase coherence in an SNS junction array of AuIn clusters, prompted apparently by the onset of superconductivity in these clusters with local T_c of 0.65 K. The observed gradual, almost linear, drop in resistance of these thicker films can only result from the presence of far-apart superconducting grains with widely varying local T_c^0, apparently the case for bumpy films prepared by fast deposition as shown in Fig. 2(c).

Films prepared by slow deposition behave differently. Two smooth films, 30 nm and 40 nm thick, prepared by slow deposition, showed two sharp drops in film resistance around 0.35 K and 0.65 K respectively [Fig. 5(a)]. Based on the above analysis, the drop at 0.65 K should correspond to the superconducting transition of grains of the AuIn phase with a superconducting transition of 0.65 K. The interesting question is whether the second drop in resistance corresponds to the superconducting transition of the AuIn phase with a T_c of 0.45 K. In this regard, annealing studies have provided some useful insight. It was found that the temperature of this second drop increased significantly after low-temperature ($< 100\,^\circ$C) annealing carried out by exposing the sample to a heat lamp for one hour in vacuum (Fig. 6). In addition, the onset T_c shifted to higher temperature, from 0.65 K to 0.70 K. The phase corresponding to an onset T_c of 0.8 K may be thermodynamically favorable. Annealing would then encourage the growth of this phase, making the film closer to the film prepared by fast deposition with similar thickness, even though no bumps were found to form as a result of the annealing.

It is striking that, while the onset T_c of *all* films fall into the neighborhood of three distinct values (0.45 K, 0.65 K, and 0.8 K), the temperatures corresponding to the second resistance drop appeared to be unsystematic. This, however, is fully consistent with the picture that the resistance drop at the lower temperature is due to the emergence of global phase coherence resulting from Josephson coupling among superconducting grains. This is further supported by the observation that the lowering of the temperature for the second resistance drop is accompanied by a significant reduction in the normal-state resistance after annealing. Indeed, it is known that the Josephson coupling in an SNS junction depends on the coherence length in the *N* layer, which in turn is reflected in the normal-state resistance of the film.

Two-step transitions were previously observed in proximity-coupled Josephson junction arrays.[7] However, because the local T_c of the superconducting islands was uniform and equal to the bulk T_c of the superconductor, the resistance dropped sharply at this temperature. In the present study, especially for the bumpy films, because of the proximity effect, the In-rich grains embedded in the $Au_{0.9}In_{0.1}$ α-phase matrix (which is a normal metal above its T_c of 77 mK) would have a local T_c dependent on their size and the exact local In concentration. Below the superconducting transition of these In-rich grains, but above that of $Au_{0.9}In_{0.1}$, the films should behave as random networks of SNS (proximity-coupled) Josephson junctions. As the temperature is lowered, a sharper transition to a zero-resistance superconducting state was observed due to the phase coherence of all superconducting grains. Obviously, the onset superconducting transition of another superconducting Au-In phase (of a lower T_c) will help bring about this global phase coherence, which seems to be the case for the thicker films prepared by fast deposition [Fig. 5(b)].

While a general trend in the relationship between the film morphology and the electrical transport properties of the film has been found, it is important to emphasize that such a relationship can be rather subtle. In Fig. 5(a), the $R(T)$ curves of two pairs of 7.5-nm- and one 10-nm-thick films are plotted. It is clear that in such small-thickness regime, the normal-state resistance, as well as the global superconducting transition temperature, depends sensitively on the evaporation rate. On the other hand, the general trend that the faster deposition results in higher normal-state resistance and lower global T_c appears to still hold.

It is interesting to note that two 20-nm-thick films prepared at $e = 0.9$ nm/s and 0.5 nm/s, respectively, have particularly wide superconducting transition regimes. This may be due to the fact that at such an intermediate thickness, neither the substrate effect nor the growth kinetics dominates. This led to films without a clearly predominant superconducting phase and a wide superconducting transition. Indeed, the 20-nm-thick film prepared by fast deposition appears to have an onset T_c between 0.65 K and 0.8 K. AFM imaging of these films revealed that, while no protruding clusters were seen, large mesas of low heights were scattered around in the films.

TABLE I. Summary of the sample characteristics of $Au_{0.7}In_{0.3}$ films discussed in this paper, including morphology ("s" for smooth films, "b" for bumpy films with protruding clusters), nominal film thickness d, average evaporation rate e, normal-state sheet resistance $R_N^{\square}$, onset temperature for superconductivity $T_c^{\rm onset}$, and zero-resistance transition temperature T_c. Actual thickness, estimated from AFM edge profiles for some films, was larger than d by several percent. $T_c^{\rm onset}$ and T_c were evaluated at the $0.99R_N$ and $0.01R_N$ resistance levels, respectively. Electrical transport measurements were not carried out for films Nos. 28 and 29, which were prepared for structural and compositional studies.

Film No.	s/b	d (nm)	e (nm/s)	$R_N^{\square}$ (Ω)	$T_c^{\rm onset}$ (K)	T_c (K)
8	b	30	0.9	4.2	0.734	0.586
9	s	20	0.8	11.5	0.669	0.378
10	b	35	1.1	3.9	0.804	0.561
11	s	25	0.7	6.4	0.767	0.561
16	s	15	0.8	34.4	0.423	0.333
17	s	10	0.6	210	0.382	0.221
18	s	7.5	0.4	89.1	0.431	0.229
19	s	5	0.5	3080	-	-
21	s	40	0.3	3.1	0.624	0.321
22	s	30	0.3	4.7	0.653	0.340
23	s	20	0.4	8.2	0.791	0.374
24	s	10	0.3	25.0	0.456	0.300
25	s	7.5	0.3	42.6	0.416	0.273
28	s	100	0.4	-	-	-
29	b	40	1.2	-	-	-

VII. NORMAL-STATE SHEET RESISTANCE AND THE EFFECT OF APPLIED MAGNETIC FIELDS

The normal-state resistivity of a $Au_{0.7}In_{0.3}$ film is typically a measure of the degree of disorder that affects electron motion in the normal state. The normal-state sheet resistance of the film can be controlled by the film thickness. In the present study, the underlying phases of films prepared by slow deposition may have been affected strongly by the details of the substrate conditions. On the other hand, the films prepared by fast deposition shown in Fig. 5(b) revealed more systematic behavior as a function of film thickness than those prepared by slow deposition and, therefore, will be the focus of this discussion.

The onset of the superconducting transitions of films prepared by fast deposition was found to be at either 0.45 K or 0.8 K, corresponding to two different Au-In phases. The zero-resistance T_c, corresponding to the onset of global phase coherence, was suppressed from about 0.6 K for the 35–40-nm-thick films to about 0.35 K for the 15-nm- and 20-nm-thick films, and finally to about 0.23 K for the 10-nm-thick film. For the 5-nm-thick film, no superconductivity was found.

The normal-state sheet resistance for the superconducting films, while varying substantially (see Table I), remained very low for all films studied. For thicker films, the values of the sheet resistance scaled with the film thickness (Fig. 7), yielding a resistivity of approximately 12 $\mu\Omega$ cm at 1 K. Even for the 5-nm-thick film, the normal-state sheet resistance was only 3 kΩ. This film remained metallic ($dR/dT>0$) down to 0.3 K, indicating that the electrons in $Au_{0.7}In_{0.3}$ films are quite delocalized. However, even the relatively thick $Au_{0.7}In_{0.3}$ films with a sharp transition to global superconductivity may possess a high degree of disorder for Coo-

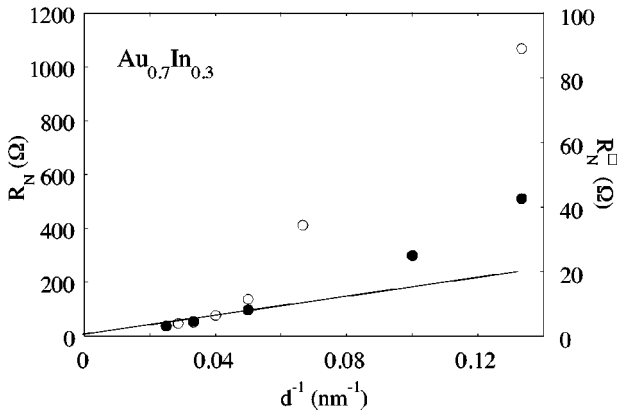

FIG. 7. Normal-state resistance, taken at $T=1$ K, plotted as a function of the inverse of the film thickness for films shown in Fig. 5. The solid circles are for films grown by slow deposition, while the open circles are for films prepared by fast deposition. The linear fit, which indicates that the thicker films have similar resistivities ($\rho=R_N^{\square}d$), corresponds to $\rho=12$ $\mu\Omega$ cm.

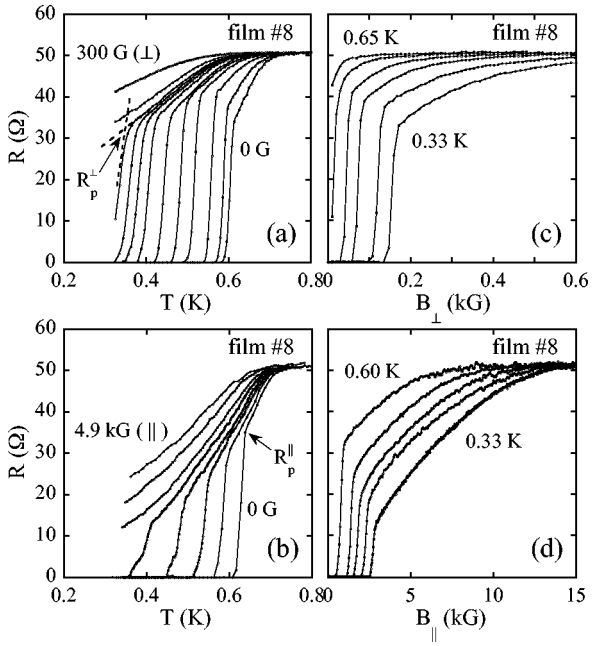

FIG. 8. Resistance of 30-nm-thick bumpy film (film No. 8), plotted as a function of temperature for different values of (a) perpendicular and (b) parallel magnetic fields and as a function of (c) perpendicular and (d) parallel field at different temperatures. For (a), from top to bottom, $B_\perp=300$, 170, 160, 150, 120, 110, 100, 75, 50, 25, 10, and 0 G. For (b), from top to bottom, $B_\parallel=4900$, 3920, 2940, 2450, 2960, 1500, 980, and 0 G. For (c), from top to bottom, $T=0.65$, 0.625, 0.60, 0.55, 0.50, 0.40, and 0.33 K. For (d), from top to bottom, $T=0.60$, 0.55, 0.50, 0.425, and 0.33 K. Measurements were carried out during two separate cooldowns. Temperatures below 0.3 K were not available for these measurements.

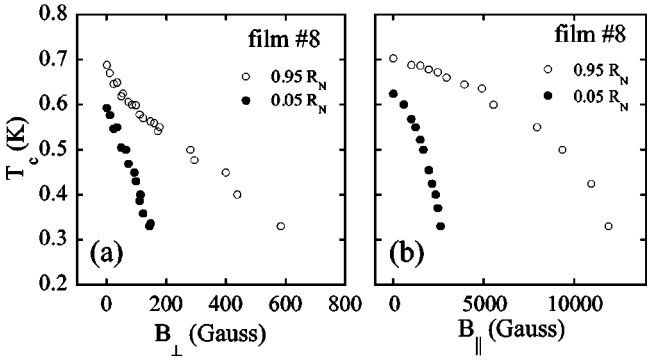

FIG. 9. Values of the onset $[R(T_c^0)=0.95R_N]$ and the global superconducting transition temperature $[R(T_c)=0.05R_N]$ plotted as a function of magnetic field in (a) perpendicular and (b) parallel directions, for film No. 8.

per pairs because of the inhomogeneity in the amplitude of superconducting order parameter. On the other hand, the normal state of these $Au_{0.7}In_{0.3}$ films is a perfectly good metal, making these films a unique superconducting system.

In Fig. 8, the results of more detailed resistance measurements are presented for the 30-nm-thick film. Perpendicular ($B_\perp$) and parallel ($B_{||}$) magnetic fields should affect the superconducting transition of the film in different ways. This was expected since $B_\perp$ created superconducting vortices in the film, which would induce a finite resistance if they were depinned and started to creep in the film. On the other hand, the effect of $B_{||}$ was primarily to suppress the superconducting gap of each individual grain via the Zeeman effect, as vortices cannot be induced in the film in this field orientation if we ignore the effects of any small misalignment. Correspondingly, a much lower $B_\perp$ than $B_{||}$ was needed to suppress the global superconducting transition.

The motion of vortices in an SNS Josephson junction array is directly related to phase slips. Enhanced phase slips due to the presence of a magnetic field, and therefore phase fluctuations, will lead to a wide superconducting transition regime (Fig. 8) and a suppressed global T_c, as shown in Fig. 9. Similar behavior was found when the film was made thinner, as discussed above. In a parallel field, while the field does not introduce free vortices to the film directly, suppressing superconductivity in the grains with a sufficiently large $B_{||}$ will lead to enhanced phase slip, which involves unbinding of a vortex-antivortex pair, again resulting in a wider superconducting transition regime. This effect is clearly illustrated in Fig. 9, where the magnetic field dependence for both the global and the onset (local) T_c is shown.

It is interesting to note that the resistance just above the drop, R_p, corresponding to the normal-state resistance of the SNS junction array showed an intriguing magnetic field dependence. It was found that R_p varied smoothly with the amplitude of the field, independent of the field orientation, as shown in Fig. 10. In addition, in small perpendicular magnetic fields, R_p was found to increase with field (Fig. 10).

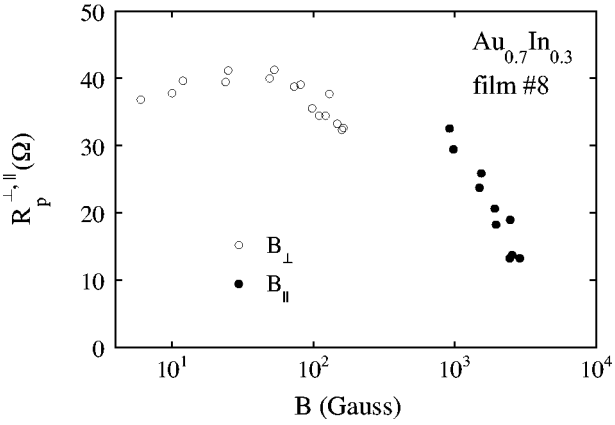

FIG. 10. Critical resistance R_p, defined as the sheet resistance right above the global superconducting transition, plotted as a function of magnetic field in perpendicular (open circles) and parallel (solid circles) directions for film No. 8.

Such a variation may provide a hint as to how the global phase coherence emerges in these bumpy films. To clarify such field dependence of R_p, more theoretical and experimental work is needed.

VIII. CONCLUSION

In conclusion, we have presented results on studies of superconducting $Au_{0.7}In_{0.3}$ films with varying thickness. The films were grown by sequential deposition and interdiffusion of multiple Au and In layers. The structural and electrical transport studies of $Au_{0.7}In_{0.3}$ films, especially the observations of the onset superconducting transition temperatures of the films, suggest the presence of several Au-In phases, including, most likely, $Au_{0.9}In_{0.1}$ ($T_c=77$ mK), two In-rich phases ($T_c=0.45$ and 0.65 K, respectively), which are likely of a composition of AuIn, and another In-rich phase with a superconducting transition at 0.8 K, forming protruding clusters in films prepared by fast deposition.

At temperatures below their onset superconducting transition temperatures, the In-rich regions became Josephson coupled with one another, resulting in a random network of Josephson junctions of SNS type, a disordered version of previously studied artificial arrays of SNS Josephson junctions. The present work has established an apparently rather unique system which is disordered as far as the Cooper paris are concerned, while the normal state remains a good metal.

ACKNOWLEDGMENTS

The authors would like to thank Vince Bojan, Mark Angelone, Tom Rusnak, and Ed Basgall of Penn State Materials Characterization Laboratory for help with characterization of the $Au_{0.7}In_{0.3}$ films. They would also like to thank Mari-Anne Rosario for discussions and help preparing the manuscript. This work was supported by the NSF under Grant No. DMR-9702661.

[1] G. Deutscher, Y. Imry, and L. Gunther, Phys. Rev. B **10**, 4598 (1974); R. C. Dynes, J. P. Garno, and J. M. Rowell, Phys. Rev. Lett. **40**, 479 (1978); B. G. Orr, H. M. Jaeger, and A. M. Goldman, Phys. Rev. B **32**, 7586 (1985).

[2] See, for example, *Percolation, Localization, and Superconductivity*, edited by A. M. Goldman and A. A. Wolf (Plenum Press, New York, 1984).

[3] M. Tinkham, *Introduction to Superconductivity*, 2nd ed. (McGraw-Hill, New York, 1996), p. 52.

[4] B. G. Orr, H. M. Jaeger, A. M. Goldman, and C. G. Kuper, Phys. Rev. Lett. **56**, 378 (1986); H. M. Jaeger, D. B. Haviland, B. G. Orr, and A. M. Goldman, Phys. Rev. B **40**, 182 (1989).

[5] For a recent review, see, for example, A. M. Goldman and N. Markovic, Phys. Today **51**(11), 39 (1998), and references cited therein.

[6] F. Zhou and B. Spivak, Phys. Rev. Lett. **80**, 5647 (1998).

[7] For a recent review, see R. S. Newrock, C. J. Lobb, U. Geigenmüller, and M. Octavio, in *Solid State Physics*, edited by H. Ehrenreich and F. Spaepen (Academic Press, San Diego, 2000), Vol. 54, p. 263.

[8] S. T. Herbert, Y. Jun, R. S. Newrock, C. J. Lobb, K. Ravindran, H.-K. Shin, D. B. Mast, and S. Elhamri, Phys. Rev. B **57**, 1154 (1998).

[9] D. C. Harris, S. T. Herbert, D. Stroud, and J. C. Garland, Phys. Rev. Lett. **67**, 3606 (1991).

[10] M. W. Johnson and A. M. Kadin, Phys. Rev. B **57**, 3593 (1998).

[11] *Phase Diagrams of Binary Gold Alloys*, edited by H. Okamoto and T. B. Massalski (ASM International, Materials Park, OH, 1987), p. 142.

[12] D. C. Hamilton, Ch. J. Raub, B. T. Matthias, E. Corenzwit, and G. W. Hull, Jr., J. Phys. Chem. Solids **26**, 665 (1965).

[13] J. H. Wernick, A. Menth, T. H. Geballe, G. Hull, and J. P. Maita, J. Phys. Chem. Solids **30**, 1949 (1969).

[14] S. Rehmann, T. Herrmannsdörfer, and F. Pobell, Phys. Rev. Lett. **78**, 1122 (1997).

[15] Ch. Buchal, R. F. Mueller, F. Pobell, M. Kubota, and H. R. Folle, Solid State Commun. **42**, 43 (1982).

[16] R. F. Hoyt and A. C. Mota, Solid State Commun. **18**, 139 (1976).

[17] H. L. Luo and K. Andres, Phys. Rev. B **1**, 3002 (1970).

[18] T. G. Finstad, T. Andreassen, and T. Olsen, Thin Solid Films **29**, 145 (1975).

[19] V. Simić and Ž. Marinković, Thin Solid Films **41**, 57 (1977).

[20] M. Seyffert, A. Siber, and P. Ziemann, Phys. Rev. Lett. **67**, 3792 (1991); Thin Solid Films **208**, 197 (1992).

[21] M. Millares, B. Pieraggi, and E. Lelievre, Solid State Ionics **63**, 575 (1993).

[22] T. Herrmannsdörfer, P. Smeibidl, B. Schröder-Smeibidl, and F. Pobell, Phys. Rev. Lett. **74**, 1665 (1995).

[23] Y. Liu, Yu. Zadorozhny, M. M. Rosario, B. Y. Rock, P. T. Carrigan, and H. Wang, Science **294**, 2332 (2001).

[24] Yu. Zadorozhny, D. R. Herman, and Y. Liu, Phys. Rev. B **63**, 144521 (2001).

[25] Yu. Zadorozhny and Y. Liu, Europhys. Lett. **55**, 712 (2001).